NMPC FOR SETPOINT TRACKING OPERATION OF A SOLID OXIDE ELECTROLYSIS CELL SYSTEM

Douglas A. Allan[ac], Vibhav Dabadghao[e], Mingrui Li[e], John C. Eslick[ac], Jinliang Ma[ac], Debangsu Bhattacharyya[d], Stephen E. Zitney[b*], Lorenz T. Biegler[e],
[a]National Energy Technology Laboratory, Pittsburgh, PA, 15236
[b]National Energy Technology Laboratory, Morgantown, WV, 26507
[c]NETL Support Contractor, Pittsburgh, PA, 15236
[d]Dept. of Chemical Engineering, West Virginia University, Morgantown, WV, 26506
[e]Dept. of Chemical Engineering, Carnegie Mellon University, Pittsburgh, PA, 15213
*steve.zitney@netl.doe.gov

Abstract

Solid oxide electrolysis cells (SOECs) are a promising technology to generate hydrogen through water electrolysis. However, intermittent renewable energy requires SOECs to transition between hydrogen production setpoints as the price of electricity fluctuates. A well-functioning control system is important to avoid cell degradation during setpoint tracking operation. In this work, we apply nonlinear model predictive control (NMPC) to an SOEC module and supporting equipment and compare NMPC performance to classical PI control while ramping between hydrogen production setpoints. We find that these control methods provide similar performance in many metrics, but NMPC significantly reduces cell thermal gradients during the setpoint transition.

Keywords

Sustainability, Implementation, Energy & Environment, Process Optimization & Control, NMPC, SOEC

Introduction

Hydrogen production may play a crucial role in the energy transition and decarbonization. Today, most industrial hydrogen is produced through steam methane reforming, which uses fossil fuels as a feedstock. Water electrolysis is a potential replacement, producing no direct greenhouse gas emissions when renewable energy is used.

For water electrolysis, the Nernst potential---the minimum potential difference at which electrolysis can occur---decreases with increasing reaction temperature. Because solid oxide electrolysis cells (SOECs) operate at 600 °C to 1000 °C, much higher temperatures than other electrolysis technologies, they are good candidates for efficient water electrolysis. However, high temperature operation comes with significant drawbacks. SOECs require additional heat exchange equipment and good thermal insulation. Transitions between operating points must be controlled carefully to minimize power requirements and avoid thermal stress.

Flexible operation is necessary to operate profitably with intermittent renewable energy but switching between setpoints risks damaging the cells. Therefore, tight controls are needed to reduce degradation during frequent transients. Cai et al. (2014) use optimal control to ramp from minimum to maximum hydrogen production in a simplified flowsheet consisting of only a compressor and an SOEC stack. Saeedmanesh et al. (2019) present a standalone SOEC flowsheet and use proportional integral (PI) controllers to control power usage to match generation from a photovoltaic cell.

* To whom all correspondence should be addressed

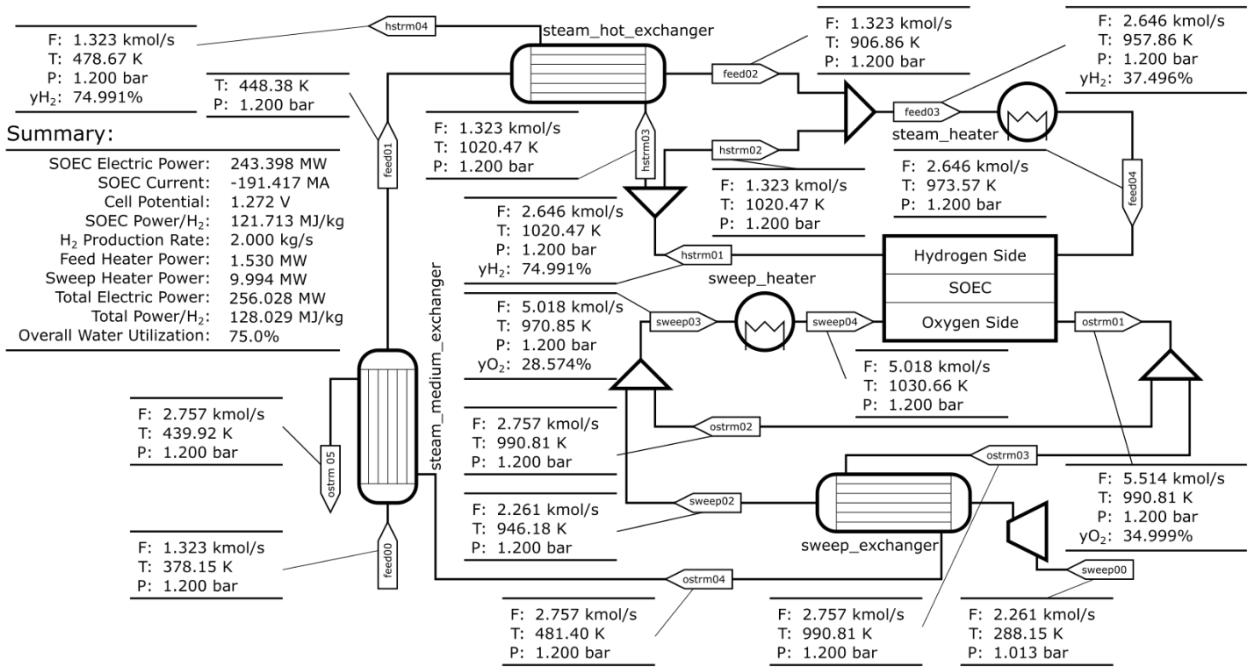

Figure 1: Process flow diagram of SOEC system

SOEC systems are good candidates for model predictive control (MPC) since many manipulated variables (MVs) are highly interactive. MPC (see (Rawlings et al., 2022) and (Raković & Levine, 2019)) is a method of advanced control that uses a system model to predict system response to a sequence of MVs and optimizes it with respect to some performance metric. Simultaneous handling of constraints where the controller can manipulate several degrees of freedom affords a quicker response than classical control.

In this paper, we apply nonlinear MPC (NMPC) to an SOEC module and supporting equipment and compare the performance of NMPC to classical PI control while ramping from a minimum hydrogen production rate of 0.4 kg/s to a maximum of 2 kg/s. Performance is judged based on the speed of production rate transition, whether safe SOEC feed and effluent concentrations are maintained, and whether unsafe temperature levels or gradients occur in the SOEC.

Process Modeling

Figure 1 shows a process flow diagram for the SOEC module and supporting equipment. The SOEC model was developed in the open-source, equation-oriented IDAES[1] (Institute for the Design of Advanced Energy Systems) modeling framework (Lee, et al., 2021). Saturated steam entering the system at 105 °C and 1.2 bar passes through two heat exchangers to absorb heat from the hot SOEC effluent streams. Air for use as a sweep gas enters at atmospheric pressure and 15 °C. This air is compressed up to the stack operating pressure of 1.2 bar, and then heated using hot sweep gas leaving the SOEC. Both the steam feed and the sweep gas streams are then mixed with the hot recycled effluent streams from the SOEC hydrogen-side and oxygen-side, respectively. They are further heated by trim heaters before entering the SOEC.

While a complete discussion of SOEC modeling and parameter estimation is beyond the scope of this paper, we provide an overview of the first-principles non-isothermal

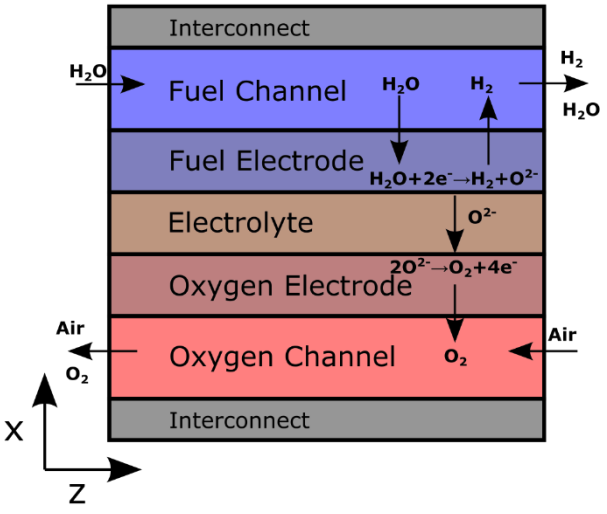

Figure 2: Schematic of SOEC model. Note that this diagram is not to scale---the cell is millimeters thick, and the electrolyte and oxygen electrode are micrometers thick.

[1] https://github.com/IDAES/idaes-pse

planar SOEC model used here (Figure 2). To avoid ambiguity in the terms "anode" and "cathode" when considering reversible SOECs, we use "fuel electrode" for the electrode in which water is reduced into hydrogen and "oxygen electrode" for the electrode to which O^{2-} ions diffuse. The default SOEC model uses one (spatial) dimensional channel sub-models with two-dimensional electrode, electrolyte, and interconnect sub-models, discretized using a finite volume method. However, many configuration options exist enabling approximations and model reduction as called for by different applications.

The core dynamic modeling equations used are given in (Bhattacharyya et al., 2007), suitably adjusted for Cartesian rather than cylindrical coordinates. However, the general form of the Butler-Volmer equation, as given by (Noren & Hoffman, 2005), is used instead of the hyperbolic sine approximation. To scale between cell-level results and module-level results, the cell material flow rates are multiplied by the number of cells in the module. Heat loss through interaction with the environment is not considered.

SOEC model parameters were chosen to match the fuel electrode-supported short stack in (Fang et al., 2015). Electrochemical parameters were determined by comparing the experimental V-I curve with model predictions. In cells built to this specification, the oxygen electrode and electrolyte combined are only 5% as thick as the fuel electrode. Therefore, those layers were reduced to thin films given specific area-squared resistance values without appreciable resistance to heat or (in the case of the oxygen electrode) mass transport. On the other hand, the interconnect in the experimental stack was 5 mm thick (probably to facilitate insertion of thermocouples, but no reason was explicitly given). A value of 2 mm was used in the cell model in this study under the assumption that cells in a production stack would have a thinner interconnect.

First-principles one-dimensional dynamic models are used for the three heat exchangers and two trim heaters. Multipass crossflow heat exchangers are used, while the trim heaters are modeled as cross flow heat exchangers with empty tubes heated through resistive heating. Material and energy balances and performance equations are included for the heat exchangers and heaters, while the mixers and splitters have only material and energy balances. The blower assumes a fixed isentropic efficiency.

Gas-phase material and energy holdups in the SOEC module and throughout the flowsheet are ignored due to their small magnitude and short gas residence times. Therefore, dynamic behavior is dominated by the thermal holdup in the metal mass of the SOEC, heat exchangers, and trim heaters. While the system is open-loop stable, the large amount of heat exchanged between SOEC feed and effluent combined with the metal mass in various units cause an open-loop setpoint transition to take nearly a week to come to steady state. Therefore, for flexible operations, a tight control system is necessary to transition between setpoints.

*Table 1: Manipulated variables and their pairings in classical control. Artificial variables marked with *.*

Controller Type	Manipulated Variable (MV)	Controlled Variable (CV)
PI	Cell potential	Water conversion
PI	Steam heater duty	Steam heater outlet temperature
PI	Sweep heater duty	Sweep heater outlet temperature
PI	Steam feed rate	H_2 production rate
None	Sweep feed rate	-
None	Steam recycle ratio	-
P	Sweep recycle ratio	SOEC sweep outlet temperature
P	Steam heater outlet temperature setpoint*	SOEC steam outlet temperature
P	Sweep heater outlet temperature setpoint*	SOEC sweep outlet temperature

Classical Process Control

A control system for the flowsheet in Figure 1 needs to transition quickly between setpoints without large spatial temperature gradients occurring in the SOEC. Several performance constraints govern stack operation. Overall conversion of steam to hydrogen should not exceed 75% to avoid steam starvation due to uneven gas distribution. Also, conversion should not drop below 75% so that the system uses steam efficiently. Hydrogen content in the feed should mostly remain above 5% (mole basis) to avoid degradation and oxygen content in the sweep outlet should mostly remain below 35% to prevent oxidation of process components. To avoid stack thermal stress, the maximum magnitude cell thermal gradient is kept below 200 K/m.

Seven manipulated variables (MVs) are available for control purposes: steam and sweep gas feed rates, steam and oxygen trim heater duties, steam and oxygen recycle ratios, and cell potential. However, there are no obvious controlled variables (CVs) to pair with many of these MVs. Cell potential has a large and immediate effect on overall water conversion, so pairing those variables is natural. Overall water conversion cannot be measured directly, but, in the absence of current leaks, it can be calculated from the steam feed rate and total SOEC module current, both of which can be easily measured. With cell potential so paired, steam feed rate can be paired with H_2 production rate. Trim heater duties can be paired with trim heater outlet temperatures to create tight control loops.

However, those pairing leave relatively few variables available for SOEC thermal management. Although the sweep flow rate and both recycle ratios impact stack temperature, they are far less impactful than trim heater duties and cell potential. Furthermore, they also impact hydrogen content in the feed and oxygen content in the sweep effluent, whose regulation is a task for which PI control is ill-suited. Therefore, cascade control is appropriate; trim heater outlet temperature setpoints should be manipulated by controllers regulating SOEC effluent temperatures.

In a typical cascade arrangement, the inner controllers regulating trim heater outlet temperature would be proportional (P) controllers while the outer controllers regulating SOEC outlet temperatures would be PI controllers to remove offset. However, simulations showed that this arrangement resulted in controllers fighting to maintain their setpoints at the expense of others. Much better results are obtained when the *inner* controllers are PI and the *outer* controllers are purely P. Finally, another P controller pairs SOEC sweep effluent temperature with sweep recycle ratio; faster setpoint transitions are obtained with acceptable transient behavior of sweep effluent oxygen fraction. The final controller pairings are given in Table 1. Anti-windup is accomplished through smooth clamping using steep logistic functions as smooth approximations to the Heaviside function (unit step function).

Nonlinear Model Predictive Control

To compare the performance of classical and advanced control strategies, an NMPC framework was developed for setpoint transition using all seven MVs shown in Table 1. The objective function contains the weighted sum of squared errors of the trajectory-tracking of H_2 production rate as well as deviations of MVs and CVs from their reference values. An additional rate of change penalty on the trim heater duties is added to prevent oscillatory trajectories.

To prevent cell thermal degradation over time, the magnitude of the temperature gradient along the cell length (z direction) is constrained to be below 205 K/m. Applying such a state inequality constraint is known to be non-robust, as perturbations in inputs can lead to an infeasible problem. To avoid this, an l_1-penalty relaxation of this constraint in (1) maintains robustness of the controller by treating it as a soft constraint with non-negative slack variables p and n, which are penalized in the objective function.

$$\frac{dT}{dz} - 205 \le p \quad \text{and} \quad -\frac{dT}{dz} - 205 \le n \tag{1}$$

The objective function is defined as:

$$\begin{aligned} f_{\text{obj}} = &\sum_{i=0}^{N} \rho_{H_2}(y_i - y_i^R)^2 + \sum_{i=0}^{N}\sum_{j\in J} \rho_j\left(u_{ij} - u_{ij}^R\right)^2 \\ &+ \sum_{i=0}^{N}\sum_{k\in K} \rho'_k(x_{ik} - x_{ik}^R)^2 + \sum_{i=1}^{N} \rho'(v_i - v_{i-1})^2 \\ &+ \rho_s \sum_{i=0}^{N}\sum_{z=1}^{z_L}(p_{iz} + n_{iz}) \end{aligned} \tag{2}$$

The first term in the objective is the sum of squared errors of the H_2 production rate, y_i, compared to its target, y_i^R at time $t = t_i$, with $\rho_{H_2} = 1$ selected as the penalty weight. The second term involves penalties on the deviation of the seven MVs, u_{ij}, from their nominal values u_{ij}^R, with $\rho_j = 0.01$ applied after scaling the terms to be $O(1)$. Also, J represents the set of MVs. Similarly, the third term penalizes the deviation of the CVs (represented by set K) from their reference trajectories. The terms are scaled to $O(1)$ and $\rho'_k = 0.01$ is selected as the penalty weight. The fourth term is the rate of change penalty on trim heater duties represented by v, and $\rho' = 0.01$ is selected as the penalty weight after scaling the terms to $O(1)$. The last term penalizes the slack variables in (1), and $\rho_s = 0.001$. N is the number of time steps in the prediction horizon.

For this study, we assume that the system state is known by the controller; in a real application, moving horizon estimation can be used to infer the system state from measurements. Using the system state, the controller uses the system model to predict the response of a given MV trajectory over the controller horizon, then optimizes the trajectory to minimize the objective function. Then the first element of the MV trajectory is injected into the system, and, at the next sampling time, the MV trajectory is re-optimized over a shifted horizon.

Simulation Results

To compare the performance of classical control and NMPC, we simulated the SOEC system ramping hydrogen production from minimum to maximum and back to minimum. The ramps were carried out over thirty minutes, with two hours for the system to settle at its new operating point after both the ramp up and down. The dynamic simulations using classical process control were conducted using the IDAES interface to the PETSc suite of differential algebraic equation (DAE) solvers (Abhyankar, et al., 2018). Because this DAE system is stiff, a variable time step implicit Euler method was used. The time step was initialized at 1 second, after which it typically grew to 5-10 seconds during the initial transient after ramping started or stopped and then to 5–10 minutes by the end of the integration interval. When anti-windup was turned on or off in the PI controllers, the timestep decreased to 0.5-1 seconds, due to the steep transition between error integrating and not integrating. The fully discretized control problem for NMPC had about 16,000 equations and variables. The studies were performed on an Intel Core i7 CPU @ 2.11 GHz processor with 24 GB memory. On average, the solution time was 35.5 seconds for a prediction horizon of 750 seconds. In each instance, the problem was solved well within the sampling time of 150 seconds.

Figure 3 compares the performance of the two control strategies. Both classical control and NMPC reach the maximum production rate of 2 kg/s and the minimum production rate of 0.4 kg/s after the thirty-minute ramps with a small amount of overshoot. They both also maintain overall steam conversion around 75% without transgressing either the 35% upper bound on sweep effluent oxygen content or the 5% lower bound on fuel feed hydrogen content. Classical control has higher peaks in the SOEC temperature gradients than NMPC, as the latter can impose these constraints while minimally affecting cell performance. However, in both cases the SOEC takes nearly two hours to settle thermally after the ramp finishes.

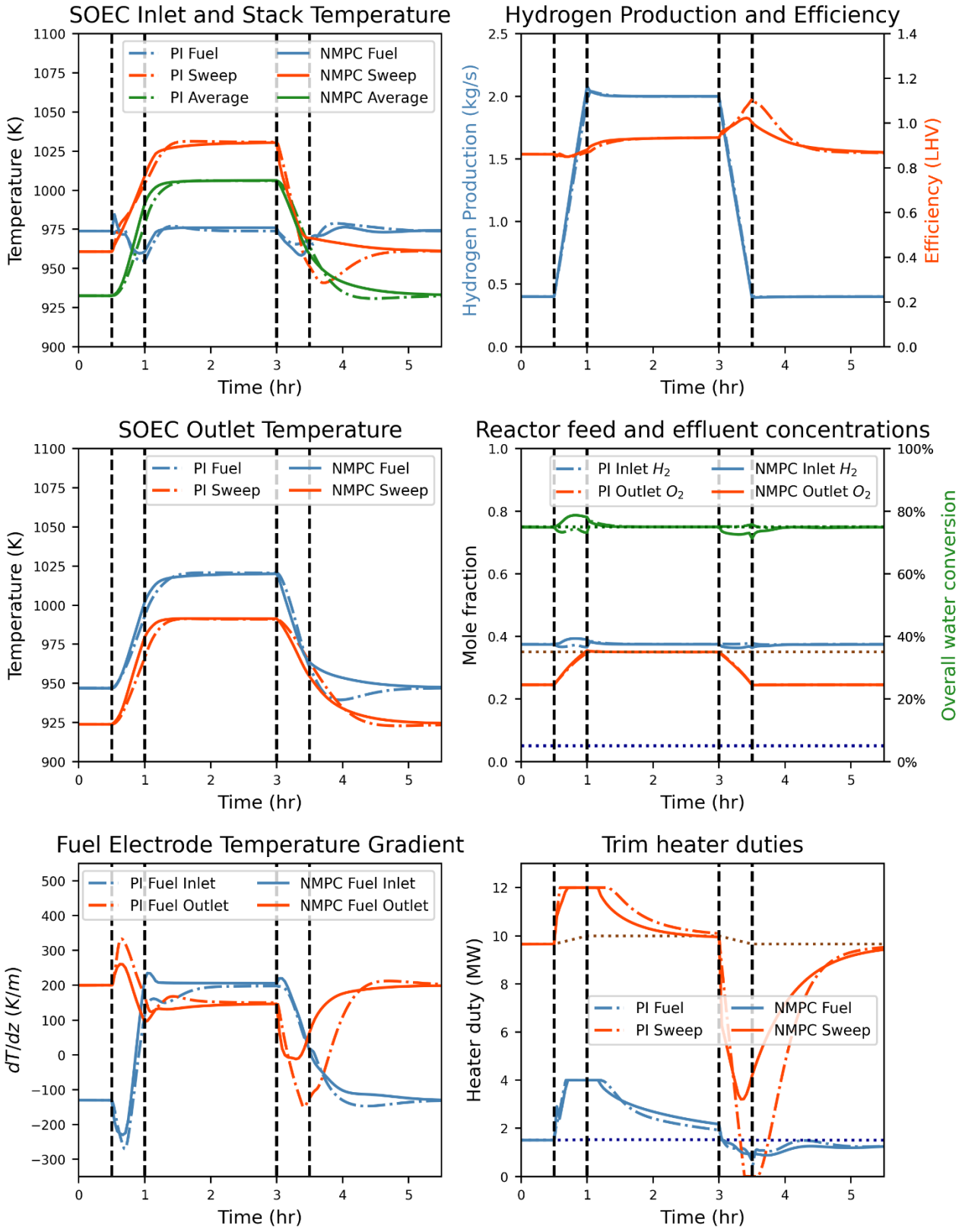

Figure 3: Comparison of classical control with NMPC. Efficiency is defined as the ratio of lower heating value (LHV) of H_2 produced to total system power consumption (i.e., not just the SOEC itself, but including trim heaters and the blower).

The trim heater duties reveal that the system is not even then at steady state, but rather the control systems are shielding the SOEC module from the slow time dynamics of the heat exchangers. Classical control is somewhat more efficient than NMPC during the ramp down, but at the cost of larger temperature gradients and a more oscillatory response.

Conclusions

A dynamic process flowsheet of an SOEC module and supporting auxiliary equipment was developed in the open-source, equation-based IDAES modeling framework. Control of this system for ramping between minimum and maximum hydrogen production rates was conducted with both classical control and NMPC. Dynamic simulation results show that while both control methods attain similar performance in several areas, NMPC can mitigate temperature gradients in the SOEC more effectively than PI.

The performance of PI control might suggest that linear MPC might control this system well. There are two major sources of nonlinearity that would hinder such an application. First, the time constants of the units in this system are dependent on the flow rate through them, and the hydrogen production rate increases by a factor of five ramping between production points. Second, the effective heat of reaction depends strongly on the cell potential. At full load, the SOEC operates near the thermoneutral point, where Joule heating in the cell provides the necessary heat of reaction for electrolysis. At minimum load, however, the SOEC is operated at a lower potential, resulting in less Joule heating and requiring the heat to be provided externally. Any linear system model would strongly depend on the operating point where the model is identified.

One factor in PI control having higher efficiency while ramping down to minimum production is that NMPC is not optimizing for efficiency, but instead for reducing the temperature gradients while tracking a setpoint. Economic MPC allows non-tracking objectives like maximizing efficiency to be used and is well-suited to this SOEC system since its response time is slow compared to the rate at which electricity prices change. Another challenge is how to manage the trade-off between operating efficiency and cell degradation; this is a topic for further research.

Acknowledgments

This work was conducted as part of the Institute for the Design of Advanced Energy Systems (IDAES) with support from the U.S. Department of Energy's Office of Fossil Energy and Carbon Management through the Solid Oxide Fuel Cell Program's Integrated Energy Systems thrust. This was prepared as an account of work sponsored by an agency of the United States Government. Neither the United States Government nor any agency thereof, nor any of their employees, nor the support contractor, nor any of their employees, makes any warranty, express or implied, or assumes any legal liability or responsibility for the accuracy, completeness, or usefulness of any information, apparatus, product, or process disclosed, or represents that its use would not infringe privately owned rights. Reference herein to any specific commercial product, process, or service by trade name, trademark, manufacturer, or otherwise does not necessarily constitute or imply its endorsement, recommendation, or favoring by the United States Government or any agency thereof. The views and opinions of authors expressed herein do not necessarily state or reflect those of the United States Government or any agency thereof.

References

Abhyankar, S., Brown, J., Constantinescu, E. M., Ghosh, D., Smith, B. F., & Zhang, H. (2018). PETSc/TS: A Modern Scalable ODE/DAE Solver Library. *arXiv e-preprints*.

Bhattacharyya, D., Rengaswamy, R., & Finnerty, C. (2007). Isothermal models for anode-supported tubular solid oxide fuel cells. *Chemical Engineering Science, 62*(16), 4250-4267.

Cai, Q., Adjiman, C. S., & Brandon, N. P. (2014). Optimal control strategies for hydrogen production when coupling solid oxide electrolysers with intermittent renewable energies. *Journal of Power Sources, 268*, 212-224.

Fang, Q., Blum, L., & Menzler, N. H. (2015). Performance and Degradation of Solid Oxide Electrolysis Cells in Stack. *Journal of The Electrochemical Society, 162*(8), F907--F912.

Lee, A., Ghouse, J. H., Eslick, J. C., Laird, C. D., Siirola, J. D., Zamarripa, M. A., . . . Miller, D. C. (2021). The IDAES process modeling framework and model library—Flexibility for process simulation and optimization. *Journal of Advanced Manufacturing and Processing, 3*(3), e10095.

Noren, D. A., & Hoffman, M. A. (2005). Clarifying the Butler-Volmer equation and related approximations for calculating activation losses in solid oxide fuel cell models. *Journal of Power Sources, 152*(1-2), 175-181.

Raković, S. V., & Levine, W. S. (2019). *Handbook of Model Predictive Control.* Birkhäuser Cham.

Rawlings, J. B., Mayne, D. Q., & Diehl, M. M. (2022). *Model Predictive Control: Theory, Computation, and Design, 2nd Edition.* Santa Barbara, CA: Nob Hill Publishing.

Saeedmanesh, A., Colombo, P., McLarty, D., & Brouwer, J. (2019). Dynamic Behavior of a Solid Oxide Steam Electrolyzer System Using Transient Photovoltaic Generated Power for Renewable Hydrogen Production. *Journal of Electrochemical Energy Conversion and Storage, 16*(4).